Experimental measurements of electron bunch trains in a laser-plasma accelerator – supplemental material

O. Lundh,[1,2] C. Rechatin,[2] J. Lim,[2] V. Malka,[2] and J. Faure[2]

[1] *Department of Physics, Lund University, P.O. Box 118, S-22100 Lund, Sweden*
[2] *Laboratoire d'Optique Appliquée, ENSTA, École Polytechnique, CNRS, 91761 Palaiseau, France*

I. LASER-PLASMA ACCELERATOR

The experiment was performed using the 10 Hz multi-terawatt Ti:sapphire laser in "salle jaune" at Laboratoire d'Optique Appliquée (LOA), which operated at a central wavelength of 820 nm. The duration of the pulses were measured to be 30 fs (FWHM) using spectral phase interferometry for direct electric-field reconstruction (SPIDER). A schematic view of the experimental arrangement is shown in Fig. 1. The experiment employed either one or two pulses. For colliding pulse injection (CPI) one pulse (pump pulse) was used to drive the plasma wave and a second pulse (injection pulse) was used to trigger injection. For self-injection (SI), only the pump pulse was used. The pump pulse, with an energy of 1.0 J, was focused using an $f = 1.0$ m focal length, on-axis spherical mirror. The focal spot was measured with a 12-bit CCD camera and was slightly elliptical, 17×22 µm at FWHM. The injection pulse, with an energy of 100 mJ, was focused using a $f = 80$ cm focal length off-axis parabolic mirror to a 25 µm (FWHM) spot. This gave an inferred intensity of 3.6×10^{18} Wcm^{-2} for the pump pulse and 1.5×10^{17} Wcm^{-2} for the injection pulse, corresponding to normalized vector potentials of $a_0 = 1.3$ and $a_1 = 0.3$ respectively. The two pulses collided at an angle of 135°, 1 mm above the center of a 3 mm diameter gas jet nozzle. Interferometric measurements of the gas jet density profile at this height revealed a 2.1 mm plateau surrounded by 700 μm gradients on each side. Helium gas was used at a backing pressures of 4, 6 and 8 bars and provided a fully ionized plasma electron density at the plateau of 7×10^{18} cm^{-3}, 10×10^{18} cm^{-3} and 13×10^{18} cm^{-3} respectively. At densities 7×10^{18} cm^{-3} and 10×10^{18} cm^{-3}, SI was very weak and CPI was used as method for injection. At density 13×10^{18} cm^{-3}, SI was dominant so the injection pulse was blocked and and only the pump pulse was used.

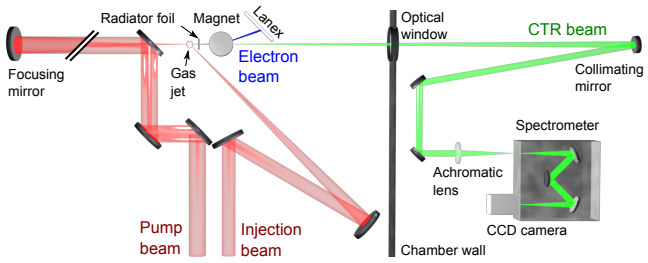

Figure 1. (Color online) Schematic view of the experimental setup.

II. CTR CHARACTERIZATION

Forward CTR was generated at the rear surface of a 100 µm Al foil which also stopped the pump laser beam. Prior to every shot, the foil was translated in order to provide unexposed material for the electron beam. The electron beam size on the foil was estimated to 90± 24 µm from the measured beam divergence. The Al foil was positioned 15 mm from the exit of the exit of the gas jet, 0.5 m from the ZnSe chamber window and 1.5 m from a 1.5 m-focal-length, spherical silver mirror which was used for light collection. For the spectral measurements, the CTR beam was focused through the slit of a Czerny-Turner imaging spectrometer (Oriel MS127i) using an $f = 200$ mm focal length, $f/4$ achromatic doublet lens. A grating with 400 lines/mm was used for dispersion and a 16-bit CCD camera (Andor DV420) was used for detection. The absolute instrumental spectral response function was determined using the manufacturer specification data, a calibrated Xe lamp, a HeNe laser and a power meter.

III. ELECTRON BEAM CHARACTERIZATION

The electron beam was dispersed by a round electromagnetic dipole, providing an effective magnetic field of 1.6 T over 25 mm. A doublet lens imaged the scintillation from a LANEX phosphor screen onto a 16-bit CCD camera (Andor DV434). The arrangement was absolutely calibrated and is described in detail in [Y. Glinec *et al.*, Rev. Sci. Instrum., **77**, 103301 (2006)]. With the magnetic field turned off and the radiator foil removed from the beam path we measure a divergence of 6.0±1.6 mrad (FWHM) and a pointing fluctuation of 2.2 mrad (RMS) for $n_e = 10 \times 10^{18}$ cm^{-3}. With the radiator in the path, we measure a divergence of 15 ± 7 mrad (FWHM). The spectral resolution was limited by the electron beam divergence. At 80 MeV it was 10% with the radiator in the path. The electron beam quality was different for the two injection mechanisms. Using SI at $n_e = 13 \times 10^{18}$ cm^{-3}, the electron beams had high charge (50 − 150 pC) and generally they were not quasi-monoenergetic, but had a large spread in the energy distribution. Using CPI at $n_e = 10 \times 10^{18}$ cm^{-3}, the electron beams had less charge (10 − 40 pC) but they were quasi-monoenergetic with peak energy in the range 80 − 120 MeV. Representative examples of beams obtained using SI and CPI are shown in Fig. 2.

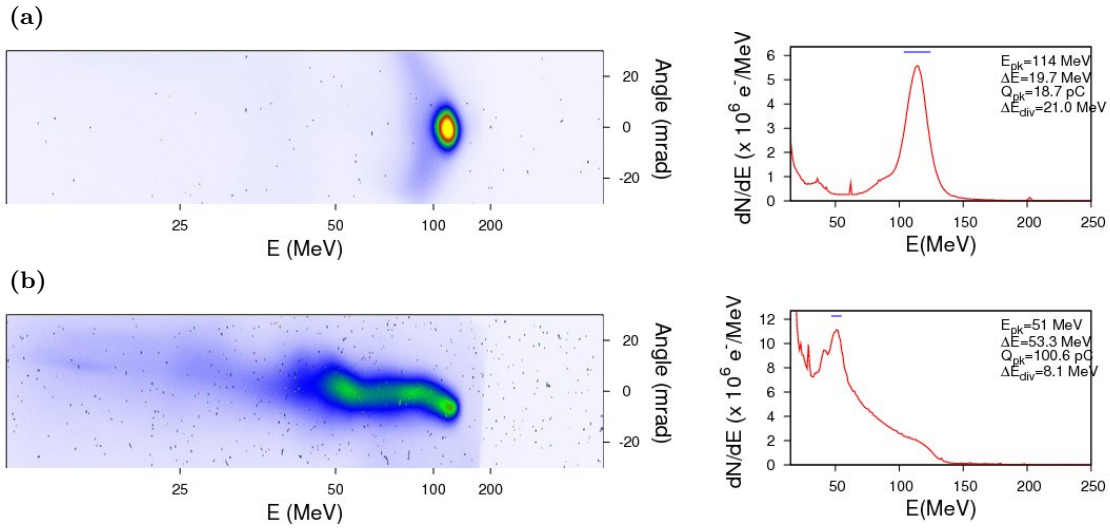

Figure 2. Representative measurements of the electron distribution using different injection mechanisms and different plasma densities, obtained with the radiator in the beam path. Left panels show the raw scintillator image. The edge of the scintillator is visible in the images as a vertical line around 180 MeV. Right panels show the electron energy spectrum. (a) Injection by colliding pulses (CPI) at $n_e = 10 \times 10^{18}\,\mathrm{W/cm^2}$. (b) Self-injection (SI) at $n_e = 13 \times 10^{18}\,\mathrm{W/cm^2}$.

IV. COHERENCE OF THE RADIATION

On the spectrometer, broadband optical radiation was observed. Null tests confirmed that the radiation was only generated if an electron beam was generated on the same laser shot. The intensity of the radiation increased with charge which is expected for transition radiation. Simultaneous measurements of the charge and the number of photons, showed that the radiation was coherent. As an example, the spectrum in Fig. 2a in the article contains $N_{ph} = 9 \times 10^6$ photons/nm at 600 nm. The electron spectrum in Fig. 2o was measured simultaneously and contained $N_e = 2.4 \times 10^8$ electrons, or 38 pC. The incoherent contribution is given by the first term in Eq. 1. At 600 nm, and for 38 pC, it is $N_{ph}^{inc} = 1.5 \times 10^3$ photons/nm within the 17 mrad half-angle of collection. This is more than three orders of magnitude below the measured number.

Another set of measurement was performed using CPI at a density of $10 \times 10^{18}\,\mathrm{cm^{-3}}$ and confirmed that the radiation was indeed coherent in the visible spectral domain. An $f = 200$ mm focal length, $f/4$ achromatic doublet lens was used to image an intermediate plane between the foil and the collecting mirror and illuminate $\sim 2.6 \times 10^4$ pixels on an absolutely calibrated 16-bit charged coupled device (CCD) camera. An interference filter in front of the camera transmitted a $\Delta\lambda = 10$ nm (FWHM) spectral band, centered at $\lambda_0 = 546$ nm. Within a 17 mrad half-angle of collection we measured a total number of $N_{ph} = 2 \times 10^7$ photons. Integration of the first term of Eq. 1 in the main article gives the total number of incoherent photons emitted by N_e electrons. For a bunch with charge 30 pC and energy 100 MeV, the incoherent contribution to the measured number of photons is $N_{ph}^{inc} = 1.3 \times 10^4$, within the solid angle of collection of the instrument. This is again three orders of magnitude below the measured number which leads to the conclusion that the radiation must be coherent.

V. VISIBILITY OF SPECTRAL MODULATIONS

In the article we argue that, if the visibility of the spectral modulations is constant with respect to wavelength, then the visibility can give an estimate of the charge ratio between consecutive electron bunches. Here we present additional evidence that, for these measurements, indeed the visibility was nearly constant over as much as one optical octave. Figure 3 shows representative examples of CTR spectra in the spectral band 500-1000 nm. For this dataset, indirectly scattered laser radiation diffusely illuminated the rear of the Al foil. Therefore, a 100 nm band around 800 nm has been masked in the data. The spectra in 3(a-i) are displayed in the wavelength domain. Both the spectral intensity and the modulation period increase as function of wavelength so variations in the visibility are difficult to determine from these plots. In the frequency domain the modulation period of the spectrum, $N(\omega)$, is constant. Therefore a smoothing cubic spline function, $S(\omega)$, was used to fit each spectrum in the frequency domain. The smoothing parameter of $S(\omega)$ was chosen such that $S(\omega)$ followed the exponentially increasing amplitude, but not the modulations. The spectra were then normalized at each frequency by dividing the spectrum by $S(\omega)$. This procedure produce a normalized and straight, modulated function, $U(\omega) = N(\omega)/S(\omega)$, shown in Fig. 3(j-r), from which it is straightforward to read the visibility as function of frequency. These examples illustrate our observation that the visibility is nearly constant (within a factor of 2) over a wide spectral range.

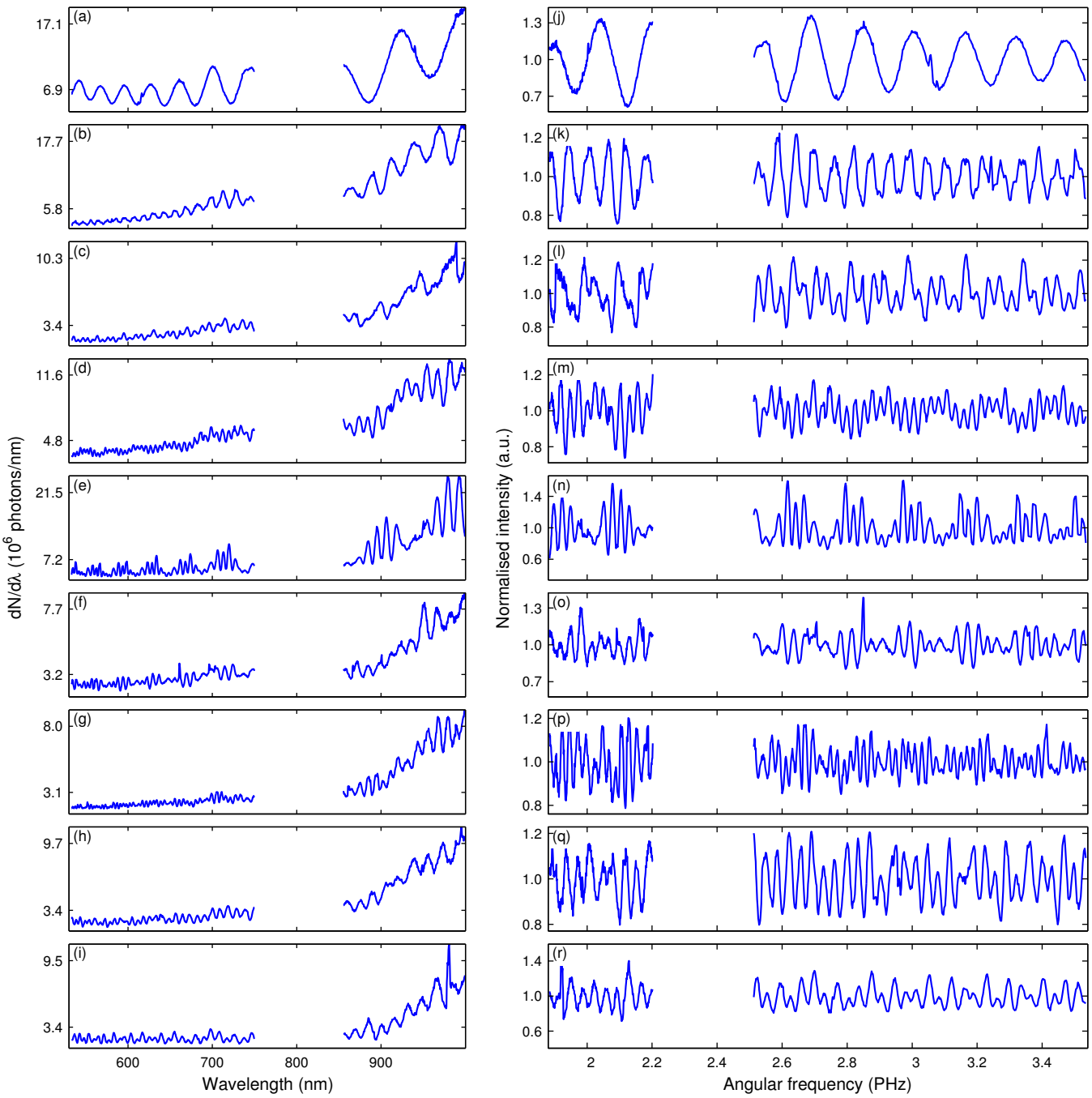

Figure 3. (a-i) Representative CTR spectra in the wavelength domain. The blank region around 800 nm has been masked because it contained scattered laser radiation. (j-r) Corresponding CTR spectra in the frequency domain, normalized and flattened by a smoothing spline interpolation as described in the text.

VI. INFLUENCE OF THE PLASMA DENSITY

The measurements of the bunch separation were performed using three plasma densities and employing either SI or CPI as methods for injection. To complement Fig. 5 in the article, a histogram for each plasma density of the quantity ct/λ_p is shown in Fig. 4. As expected, the peaks are clustered around integer numbers.

VII. INLUENCE OF ENERGY SPECTRUM

The energy spectrum influences the angular distribution of the transition radiation. In the small, on-axis solid angle that is collected by the spectrometer, the low energy part of the spectrum does not contribute much to the coherent radiation. This is illustrated in Fig. 5, which shows the results from analytical calculations of CTR. The case of 4 consecutive electron bunches is considered, with 2.5 fs duration (at FWHM) and Lorentzian shape. The first bunch has a charge of 23 pC and the trailing bunches contain 3 pC each, producing a total of 30 pC. The trailing bunches are positioned 10, 20 and 50 μm behind the first bunch. The energy distribution is peaked at 100 MeV but three different cases are considered: A) a purely mono-energetic distribution, B) a peaked distribution with 20 MeV energy spread and C) a peaked distribution with 20 MeV energy spread and a thermal background with a 40 MeV temperature. The CTR produced in case A and B is identical. The effect of a thermal background (case C) is a reduction in the number of photons, but the spectral shape is not influenced. In all cases, the total charge is 30 pC. Therefore, the peak around 100 MeV contains less charge in case C than for the other two cases. This leads to a reduction in the number of photons collected by the spectrometer.

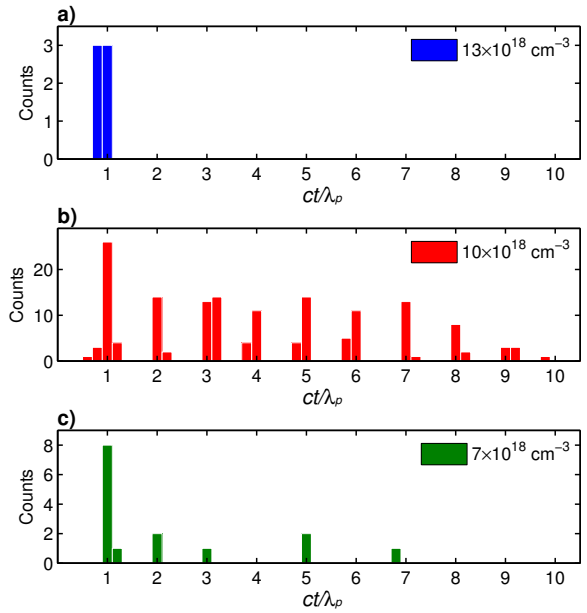

Figure 4. Distribution of ct/λ_p for different densities using a bin width of 0.2. (a) $n_e = 13 \times 10^{18}$ cm^{-3} and $\lambda_p = 9.3$ μm. (b) $n_e = 10 \times 10^{18}$ cm^{-3} and $\lambda_p = 10.6$ μm. (a) $n_e = 7 \times 10^{18}$ cm^{-3} and $\lambda_p = 12.5$ μm.

VIII. EFFECTS OF TIME-OF-FLIGHT

In general, the electron beams produced by CPI were quasi-monoenergetic with some energy spread. Electrons with different energies propagate at different speed and their separation will therefore change during propagation to the radiator, possibly influencing the measurements. However, simple estimates show that this effect is neglible. Consider two electron bunches, with significantly different energies, 60 MeV and 120 MeV respectively. When the two bunches arrive at the radiator, 15 mm from the gas jet, their separation has increased by maximum 0.4 μm. The bunch separations considered here are of the order 10–100 μm and the effect of increasing inter-bunch separation due to time-of-flight is probably not measureable under the present conditions.

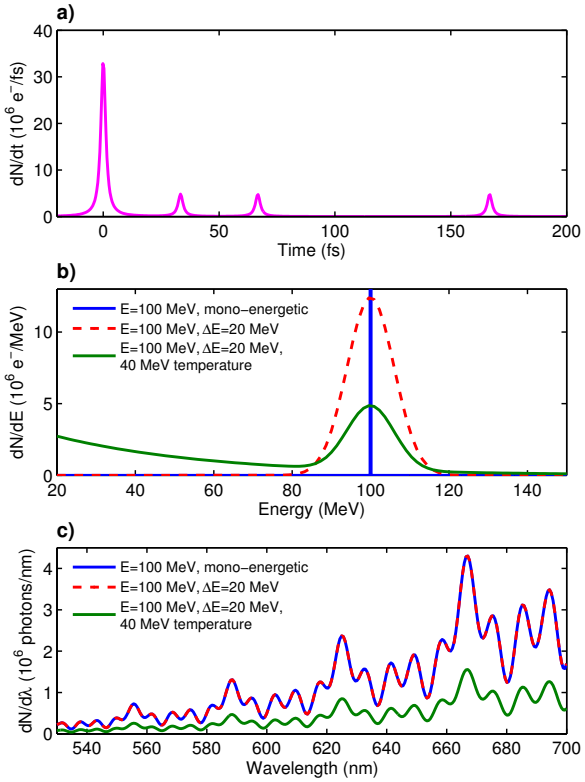

Figure 5. Effect of energy spread and a thermal background in the energy distribution. (a) Temporal distribution for all cases. (b) Energy distributions for case A (solid blue line), B (dashed red line) and C (solid green line). (c) Resulting transition radiation spectra for case A, B and C. The total charge is 30 pC in all cases.